Turbulent transport in a toroidal magnetized plasma

2012 Plasma Phys. Control. Fusion 54 085017

(http://iopscience.iop.org/0741-3335/54/8/085017)

Plasma Phys. Control. Fusion **54** (2012) 085017 (17pp) doi:10.1088/0741-3335/54/8/085017

Turbulent transport in a toroidal magnetized plasma

L Fattorini[1], Å Fredriksen[2], H L Pécseli[3], C Riccardi[1] and J K Trulsen[4]

[1] Dipartimento di Fisica 'G. Occhialini' and Università degli Studi di Milano – Bicocca, Piazza della Scienza 3, I-20216 Milano, Italy
[2] Department of Physics and Technology, University of Tromsø, N-9037 Tromsø, Norway
[3] Physics Department, University of Oslo, PO box 1048 Blindern, N-0316 Oslo, Norway
[4] Institute of Theoretical Astrophysics, University of Oslo, PO box 1029 Blindern, N-0315 Oslo, Norway

E-mail: hans.pecseli@fys.uio.no

Received 5 March 2012, in final form 16 May 2012
Published 3 July 2012
Online at stacks.iop.org/PPCF/54/085017

Abstract
Turbulent plasma transport due to low-frequency electrostatic fluctuations in a toroidal plasma is studied experimentally. The data are obtained in a magnetized toroidal plasma with no toroidal transform. The plasma is generated by a discharge from a hot electron emitting filament and diagnosed by conventional Langmuir probes measuring densities by electron or ion saturation currents and floating potentials. We present results for the statistical properties of the fluctuating radial transport caused by low-frequency electrostatic turbulence in the device. The turbulent plasma flux is identified as the product of the fluctuating density and the $\boldsymbol{E} \times \boldsymbol{B}/B^2$-velocity. Even though the probability densities of the fluctuating electric fields and plasma densities are close to Gaussians, we find strongly intermittent features in the flux signal obtained as the product of these two fluctuating quantities. A conditional statistical analysis gives insight in detail of the turbulent transport. The intermittency studies are extended by analyzing the excess statistics, i.e. the average duration of time intervals in the flux signal spent above a given reference level. We find that this analysis offers a very effective measure for intermittency effects. In our case, the signal is characterized by an excess of temporally narrow, large amplitude bursts, when compared with an equivalent Gaussian random signal.

(Some figures may appear in colour only in the online journal)

1. Introduction

Turbulent transport of magnetized plasma is important in nature as well as in many laboratory experiments [1, 2], fusion related studies in particular [3, 4]. The dominant mechanism is in many cases found to be transport by low-frequency electrostatic waves that are strongly magnetic field aligned, i.e. flute like. When all characteristic frequencies are below the ion cyclotron frequency, $\omega \ll \Omega_{ci} \ll \omega_{ce}$ we can associate the fluctuating cross-field plasma velocity with the $\boldsymbol{E} \times \boldsymbol{B}/B^2$-velocity and the time varying plasma flux becomes $\boldsymbol{\Gamma} = n\boldsymbol{E} \times \boldsymbol{B}/B^2$. We introduced the ion and electron gyro-frequencies as Ω_{ci} and ω_{ce}, respectively. With $\langle\omega\rangle$ being an average frequency in the turbulent spectrum, the polarization drift is of the order of $(\langle\omega\rangle/\Omega_{ci})E/B$, and will be ignored here. Both the electric field $\boldsymbol{E}$ and plasma density n has a dc and a fluctuating component, while we consider the externally imposed magnetic field $\boldsymbol{B}$ to be constant in time. We assume quasi-neutrality and take $n = n_e \approx n_i$ in the expression for the plasma flux.

The turbulent flux as observed in the present as well as many other experiments constitutes a random process with significant deviations from Gaussian statistics [1, 5]. In this study we analyze data from the Blaamann toroidal device at the University of Tromsø with plasma conditions as described before [6–8]. The results presented here cover a detailed statistical analysis of the radial plasma flux signal at different positions in the plasma column. For the ensuing analysis we use a local Cartesian $\{x, y, z\}$-coordinate system with $\widehat{\boldsymbol{z}} \parallel \boldsymbol{B}$ and $\widehat{\boldsymbol{x}}$ in the direction of the major radius. The origin $\{x, y, z\} = \{0, 0, 0\}$ is taken to be in the center of a circular cross-section (with minor radius r_0) of the toroidal vacuum chamber. By a radial direction we will mean a direction with respect to the origin of the local Cartesian coordinate system in

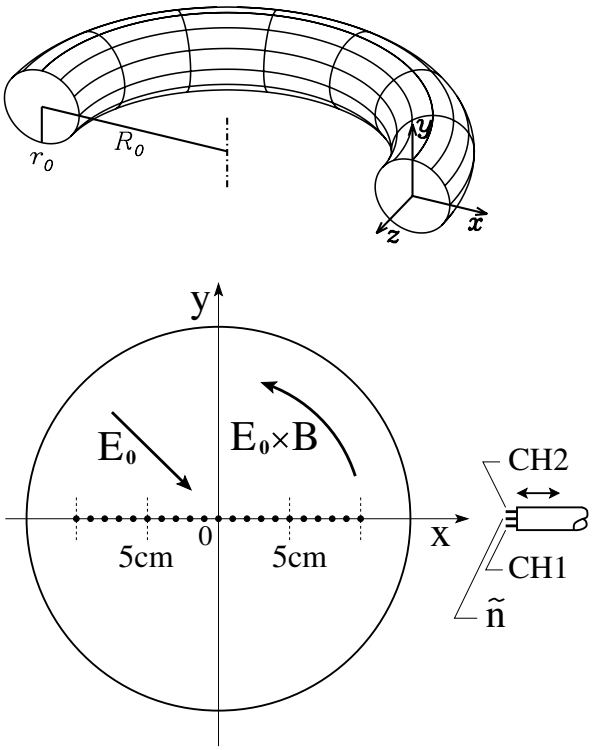

Figure 1. Sketch of a cut through the Blaamann experiment (top). The major, R_0, and minor, r_0, radii are to scale. The bottom figure shows probe positions, and the moving probe, schematically. The electric field is obtained by the potential difference from probes CH1 and CH2 on the movable probe. Positions for data acquisition are shown with small filled circles along the x-axis. We have chosen an orientation of the device where the magnetic field is directed along the positive z-axis.

the $\{x, y\}$-plane, and the term 'azimuthal direction' will refer to motions in this $\{x, y\}$-plane, see also figure 1.

We give particular attention to one feature of the fluctuating flux signal component $\Gamma_x(x) \equiv \widetilde{n}(x)\widetilde{E}_y(x)/B(x)$ with $\widetilde{E}_y$ being the fluctuating vertical electric field component at $y = 0$, while the plasma density is composed of a time averaged and a fluctuating quantity, $n = \overline{n}+\widetilde{n}$. Note that $\Gamma_x(x)$ contains both a dc and a fluctuating part. We do not consider the flux component $\overline{n}(x)\widetilde{E}_y(x)/B(x)$ that vanishes upon time averaging. Taking, for instance, a spatial position with $x > 0$, we have an outward going flux (i.e. $\Gamma_x > 0$) both when $\{\widetilde{n} > 0; \widetilde{E}_y > 0\}$ and also when $\{\widetilde{n} < 0; \widetilde{E}_y < 0\}$, so the flux signal does not distinguish between these two cases, while the physical features are in general different for the two conditions [9]. We distinguish the two cases by a conditional analysis, imposing conditions on the fluctuating $\widetilde{n}$ and $\widetilde{E}_y$ signals while analyzing the Γ_x signal. This type of analysis forms one extension of the often applied conditional averaging [10–16]. Most relevant studies are based on statistical averaging, but in some cases it has been possible to observe the spontaneous formation and propagation of individual structures [17–20], and also by external excitation [21, 22].

Intermittency studies were seemingly initiated by investigations of neutral fluid turbulence, but intermittency effects have been studied also in turbulent plasmas. In particular in fusion plasma studies it has been found that intermittency effects are often related to anomalous turbulent transport [23–25], an observation also supported by earlier laboratory studies [5]. Intermittency effects have been recognized in several different laboratory plasma devices [7, 26–28]. In order to analyze the intermittent features of the flux signal we suggest the use of excess statistics, i.e. a study of the duration of time intervals where the flux exceeds some prescribed threshold level.

In the presentation of this paper we first discuss results that can be derived from the flux density probability function $P(\Gamma_x)$. The extension of the analysis to include excess statistics requires, in general, knowledge of the joint probability distribution $P(\Gamma_x, \Gamma'_x)$ of the time varying flux component $\Gamma_x(t)$ and its time derivative $\mathrm{d}\Gamma_x(t)/\mathrm{d}t \equiv \Gamma'_x$. The conditional averages that conclude our analysis contain in general information from higher order correlations [29]. We have, as mentioned, $\langle\Gamma_x(t)\rangle \neq 0$ in general, but note that $\langle\mathrm{d}\Gamma_x(t)/\mathrm{d}t\rangle = 0$.

The paper is organized as follows: In section 2 we present some basic features of the experimental set-up. In many ways this is standard for the Blaamann plasma, so we give only a summary of the basic features for completeness. In section 3 we give details of the fluctuations generated spontaneously in the device. These depend strongly on the plasma conditions, and since they are important for the ensuing analysis, we present the results in some detail, also because parts of the analysis have not been given before for this device. The data on the turbulent fluxes form the basis of our study, and the flux signal is discussed in section 4. The intermittency analysis emphasizing the non-Gaussian features of the signal are presented in section 5. This section contains our most significant new results concerning the excess statistics of the turbulent flux in the Blaamann device. Intermittent features in plasma turbulence are often discussed in terms of conditional averaging. In section 6 we present such a study of the present data, including also new results on 'cross-conditioning', where the conditions are imposed on one set of data, while the averaging is carried out on other data combinations. After the first use of conditional averaging in plasma devices [5, 10], the method was applied in many other experiments as well. In section 7 we make a brief comparison with results from other related experiments in cases where they seem particularly relevant for the present analysis. Section 8 contains our conclusions.

The aim of this study is a detailed analysis of the turbulent flux signal and its components. The plasma instability causing the turbulent fluctuations will not be discussed here.

2. Experimental conditions

The experimental data were obtained in the Blaamann toroidal device at the University of Tromsø, where a magnetized plasma is produced by discharge from a hot filament [30]. A steady-state operation is achieved where we have a balance between plasma generation and losses, although we note that the steady-state conditions should here be understood in an averaged sense [30, 31]. The major radius of the toroidal vacuum vessel is $R_0 = 0.67$ m and the minor radius $r_0 = 0.135$ m. In figure 1

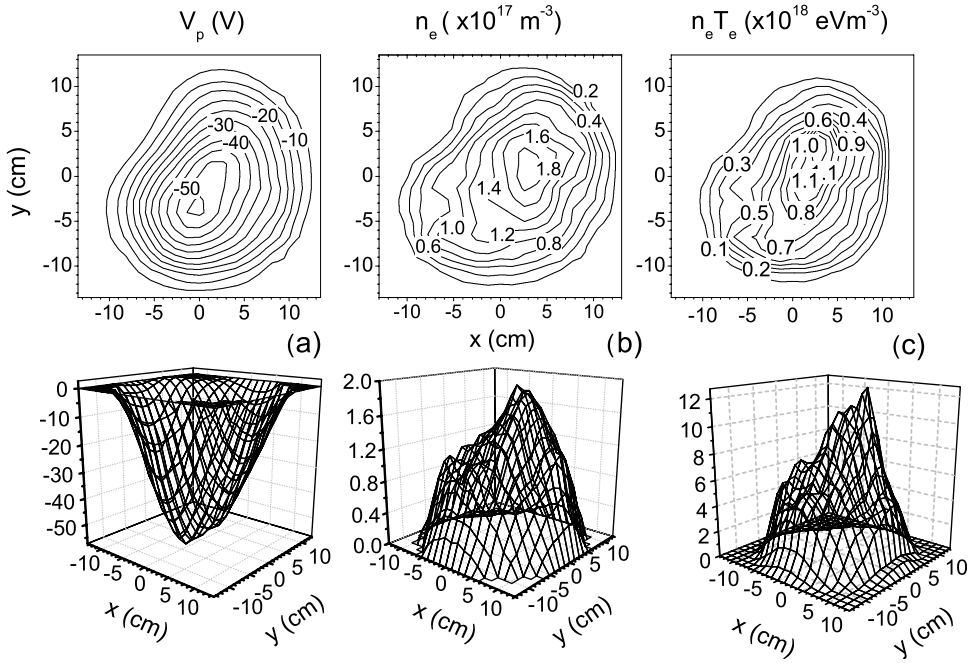

Figure 2. The dc plasma potential V_p, the dc plasma density n_e, and the dc thermal energy density $n_\mathrm{e}T_\mathrm{e}$ for a cross-section of the plasma. The narrow vertical region of enhanced electron temperature is close to the filament position. We use a local orthogonal $\{x, y, z\}$-coordinate system with $\widehat{z} \parallel \boldsymbol{B}$ and $\widehat{x}$ in the radial direction, taking the origin $\{x, y, z\} = \{0, 0, 0\}$ to be in the center of a circular cross-section of the toroidal vacuum chamber, see figure 1.

we show a sketch of the experiment also with positions for the data acquisition, where a more detailed figure is found elsewhere [30]. The plasma forms a negative potential well near the center of the vacuum vessel's circular cross-section, and is subject to vertical ∇B and curvature drifts, and azimuthal $\boldsymbol{E} \times \boldsymbol{B}$-drifts due to the radial electric field. The degree of ionization is typically ∼1%. There is no toroidal current nor poloidal magnetic fields imposed on the plasma, and hence no poloidal transform. A small vertical magnetic field can be imposed by external coils. The present experiment [7] was carried out in helium gas at a pressure of 1.0×10^{-3} mbar and a discharge current of approximately 1 A. The toroidal magnetic field was 1540 G at a reference position in the center of the vacuum vessel (at $\{x, y, z\} = \{0, 0, 0\}$ in figure 1), and the hot filament was biased at 140 V with respect to the walls. The hot filament emits electrons in abundance, and the plasma is electron rich, with a deep negative, almost parabolic dc potential profile. The plasma conditions depend on the imposed potentials and magnetic fields [8]. A summary of the spatial variation of some basic parameters is given in figure 2. For the present conditions, the almost parabolic plasma potential is a consequence of the plasma production and the magnetic field configuration: with other experimental conditions such a profile can be obtained by externally imposed potentials on hot filaments [32].

Data were acquired with a three pin Langmuir probe movable along a line crossing the center of the circular cross-section of the confining vessel [8]. The separation between the probe pins detecting the poloidal electric field fluctuations was 7 mm, each pin having a diameter of 0.25 mm, and an exposed length of 5 mm. In this experiment, the electron saturation current I_sat^- was used to represent the density fluctuations, as it gives basically the same results as we obtained from the ion saturation current from a floating double probe. The signals were digitized with a 12 bit digitizer at a sampling rate of 250 kHz (i.e. a sampling time of $\Delta t = 4 \times 10^{-6}$ s) and 10^4 samples per channel.

The dc and fluctuating densities as detected by a Langmuir probe can be assumed to represent point measurements, to a good approximation. The spatial resolution of the electric field component is, however, not ideal. Given the probe separation $2\Delta_y = 7$ mm, we detect differences in floating potentials and have the estimate for the y-component of the local electric field

$$\widetilde{E}_y(x, y) = -\left(\frac{\phi(x, y + \Delta_y) - \phi(x, y - \Delta_y)}{2\Delta_y}\right) = -\int \mathrm{i}k\widehat{\phi}(x, k)\, \mathrm{e}^{\mathrm{i}ky}\, \frac{\sin(k\Delta_y)}{k\Delta_y}\, \mathrm{d}k, \qquad (1)$$

ignoring here the z and t-variations. We use the symbol $\widehat{\phi}(k, x)$ for the Fourier transform of the electrostatic potential with respect to the y-variable. For $k\Delta_y \ll 1$ the potential difference approximates the true value of $\widetilde{E}_y$ well, but for scale sizes of the order of $2\Delta_y$ or smaller the filtering by $\sin(k\Delta_y)/(k\Delta_y)$ in (1) becomes effective [33] and the field estimate becomes inaccurate.

The full cross-section of background dc plasma parameters were obtained by a movable 2D-probe. Peak values of the time-averaged densities were $n_0 \approx 2 \times 10^{17}\,\mathrm{m}^{-3}$. Peak electron temperatures were $T_{\mathrm{e}0} \approx 6$ eV and the local minimum of the time-averaged plasma potential was $\phi_0 \approx -50$ V, see figure 2. A summary of basic plasma parameters is given in table 1. In figure 3 we show a potential cross-section along the line sampled by the movable probe, where we also show the $\boldsymbol{E}_0 \times \boldsymbol{B}/B^2$ rotation velocity of the plasma column. In

Table 1. Summary of basic plasma parameters, assuming singly charged Helium ions.

Electron plasma frequency, ω_{pe}	$1.8 \times 10^{10}\ s^{-1}$
Electron Debye length, λ_{De}	50×10^{-6} m
Reference electron temperature, T_e	5 eV
Ion temperature, T_i	0.05 eV
Sound speed, C_s	$11 \times 10^{3}\ m\,s^{-1}$
Electron thermal velocity, u_{the}	$0.94 \times 10^{6}\ m\,s^{-1}$
Ion thermal velocity, u_{thi}	$10^{3}\ m\,s^{-1}$
Electron cyclotron frequency, ω_{ce}	$27 \times 10^{9}\ s^{-1}$
Ion cyclotron frequency, Ω_{ci}	$3.7 \times 10^{6}\ s^{-1}$
Average electron Larmor radius	35×10^{-6} m
Average ion Larmor radius	0.27×10^{-3} m
Ion–electron collision frequency, $\nu_{e,i}$	$80 \times 10^{3}\ s^{-1}$
Electron–neutral He cross-section, $\sigma_{e,n}$	$6 \times 10^{-20}\ m^2$
Ion–neutral He cross-section, $\sigma_{i,n}$	$65 \times 10^{-20}\ m^2$
Electron–neutral mean free path, $\ell_{e,n}$	0.7 m
Ion–neutral mean free path, $\ell_{i,n}$	64×10^{-3} m
Electron–He collision frequency, $\nu_{e,n}$	$1.4 \times 10^{6}\ s^{-1}$
Ion–He collision frequency, $\nu_{i,n}$	$16 \times 10^{3}\ s^{-1}$

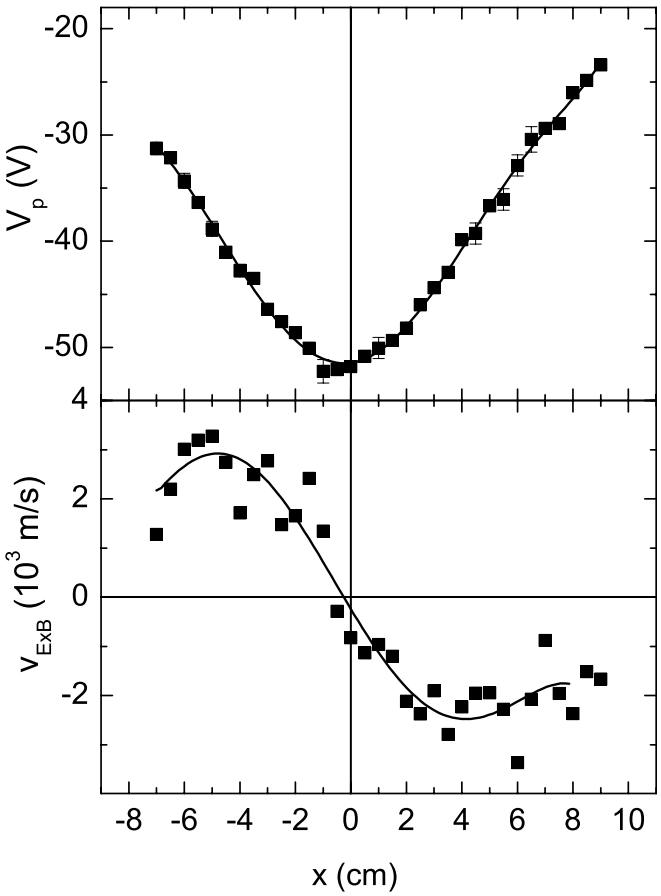

Figure 3. The experimentally obtained variation of the dc plasma potential V_p with x along a line crossing the center of the device, together with the $\boldsymbol{E}_0(r) \times \boldsymbol{B}(r)/B^2(r)$ angular rotation velocity deduced from the potential, taking into account also the magnetic field variations with $\boldsymbol{r}$.

calculating this velocity we take into account the variation of the magnetic field with r. For small r we find that the rotation velocity increases close to linearly with r, indicating a solid body rotation there. For larger radii the rotation velocity

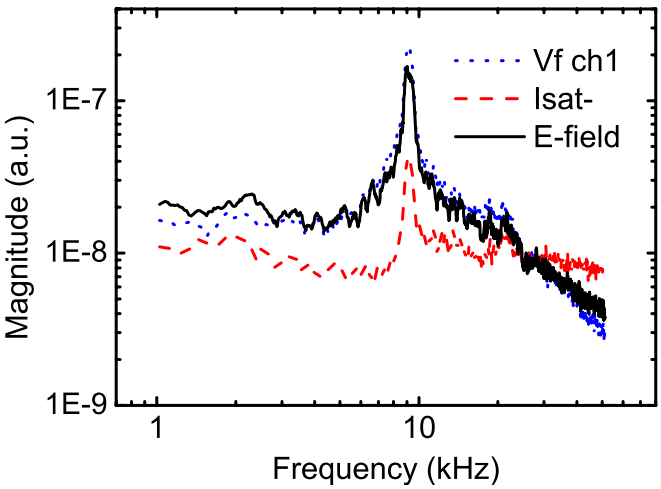

Figure 4. Root-mean-square of power spectra for fluctuations in density (Isat-), potential (Vf at ch1, see figure 1) and electric field (E-field) shown on double-logarithmic scales. The spectra are normalized to have equal integrated power over the full frequency range, up to the Nyquist frequency. The figure shows only a restricted low-frequency part of the spectrum. Note the peak in the spectrum near 10 kHz. Due to the mixing of the density and electric field oscillations, the signal for the plasma flux (not shown) contains a strong second harmonic of the peak observed here.

flattens out, and we have a shear in the cross-field angular velocity that can contribute to a Kelvin–Helmholtz type plasma instability [5, 34].

A spatially averaged radial electric field component $E_0(r)$ gives rise to a rotation of the entire plasma column. Assuming a parabolic potential and a homogeneous magnetic field given by its value at the center of the device, we estimate here a rotation frequency $\Omega_0/2\pi \approx 8 \times 10^3$ Hz. The power spectra (see figure 4) show a local peak close to this frequency. Even with these simplifying assumptions, the rotation frequency of the ions Ω_+ deviates from Ω_0, and can be found as a solution of

$$\left(1 + 2\frac{\Omega_+}{\Omega_{ci}}\right)\left(\frac{\Omega_0}{\Omega_{ci}} - \frac{\Omega_+}{\Omega_{ci}} - \left(\frac{\Omega_+}{\Omega_{ci}}\right)^2\right) = \left(\frac{\nu_{i,n}}{\Omega_{ci}}\right)^2 \frac{\Omega_+}{\Omega_{ci}}, \quad (2)$$

where the right-hand side accounts for the collisional friction with a stationary neutral gas, while the other terms include the effects of the centrifugal forces on the ions [32, 35, 36]. In principle we have a similar expression for the electrons, but with the given parameters (see table 1) we can assume from the outset that the electrons rotate with Ω_0, and ignore friction and centrifugal forces here.

If we consider a localized plasma density enhancement or depletion δn at some finite radial position, this perturbation will be polarized due to the charge separation caused by the differential electron–ion rotation. Electric fields develop that cause radial motion of the density perturbation, with density depletions and enhancements propagating in opposite directions. To estimate the polarization of a local plasma density perturbation created at some time $t = 0$, we take the difference in the angular rotation of electrons and ions $\Delta\Omega \approx \Omega_0 - \Omega_+$ and find a relative displacement of the electrons and ions to be approximately $tr\Delta\Omega$ for a density

perturbation δn localized at the position r. Apart from a numerical factor of order unity, the resulting localized electric field is then $E \approx t\, e\, \delta n\, r \Delta\Omega/\varepsilon_0\varepsilon_r$, where ε_r is the relative dielectric constant. Taking the standard form for flute type, slow plasma variations, $\varepsilon_r \approx 1 + \delta n\, Mc^2\mu_0/B^2$, we have two limits; for large density perturbations we have $\varepsilon_r \approx \delta n\, Mc^2\mu_0/B^2$, while for small densities $\varepsilon_r \approx 1$. (We have to modify ε_r when collisions are abundant.) For the first large density case we find a radial velocity of the density perturbation $E/B \approx tr\,\Omega_{ci}\Delta\Omega$ independent of density, noting that the position varies with time, i.e. $r = r(t)$. In the other limit we find $E/B \approx tr\,\delta\Omega_{pi}^2\,\Delta\Omega/\Omega_{ci}$ with $\delta\Omega_{pi}^2 \equiv \delta n e^2/M\varepsilon_0$. Taking a perturbation $\delta n/\overline{n} \approx 0.1$ at a position $x = 50$ mm, we find $\varepsilon_r \approx 300$, so the first case is relevant in the central parts of the plasma.

With parameters from table 1 we find that both $\Omega_0/\Omega_{ci} \ll 1$ and $\nu_{i,n}/\Omega_{ci} \ll 1$, and it might be tempting to ignore also the slippage between the ion and electron rotations. Indeed, it can be concluded that the difference in rotation velocities of the electrons and ions contribute only little to the azimuthal current. The polarization of a localized density perturbation can, however, become important since it increases with time. To estimate this polarization we make a series expansion from the solution of (2) to find $\Omega_+ \approx \Omega_0 - \Omega_0^2/\Omega_{ci} - \Omega_0(\nu_{i,n}/\Omega_{ci})^2$, giving $\Omega_{ci}\Delta\Omega \approx \Omega_0^2 + \Omega_{ci}\Omega_0(\nu_{i,n}/\Omega_{ci})^2$, where the last term is small with parameters from table 1. We therefore have $E/B = \mathrm{d}r/\mathrm{d}t \approx tr\,\Omega_0^2$ with solution $r(t) = a\exp\left(\frac{1}{2}\Omega_0^2 t^2\right)$ where $a = r(0)$. This result indicates that a density perturbation can propagate significant radial distances during one rotation of the plasma column. In a fixed frame, the density perturbation will appear to follow a spiralling orbit. Also the ∇B-drift will contribute to the polarization of a local plasma density enhancement or depletion. To estimate the relative magnitude of the two polarizations we compare the ∇B-velocity $u_{the}^2/(\omega_{ce}R_0) \approx 1.3 \times 10^2\,\mathrm{m\,s^{-1}}$ with $r\Delta\Omega \approx 2.5 \times 10^2\,\mathrm{m\,s^{-1}}$, where we used $R \approx R_0$ for estimating the ∇B-velocity and $r \approx 50$ mm for the differential rotation velocity. Other parameters were taken from table 1. The two polarization effects seem to be of the same order of magnitude, but the ∇B-drift is in the positive x-direction on both the low and high magnetic field sides, i.e. in the positive x-direction, and is therefore partially compensated by the plasma rotation. The polarization due to the differential rotation gives a drift that is always in the radial direction. We also note that a collisional drag will reduce the effect of the ∇B-drift, while it will increase the differential rotation, see (2).

3. Spontaneous fluctuations in the toroidal plasma

Low-frequency electrostatic fluctuations are excited spontaneously in the toroidal plasma [30, 31] and have been studied experimentally in some detail [37, 38]. A fluctuating component with a well-defined frequency is generally assumed to be an interchange mode [38] where the frequency is determined by the plasma rotation. The plasma rotation will generally not be entirely uniform and a shear in the angular rotation can modify the most unstable mode [5, 34], as already mentioned. In figure 4 we show spectra for fluctuations in potential, density and electric field obtained at the reference position. We note that the spectra for density and potential are very different: this demonstrates that the electrons have no time to adjust to a local isothermal equilibrium (in which case we would have $e\tilde{\phi}/T_e \approx \tilde{n}/\overline{n}$ at all frequencies), consistent with the flute-like features of the dominant fluctuations.

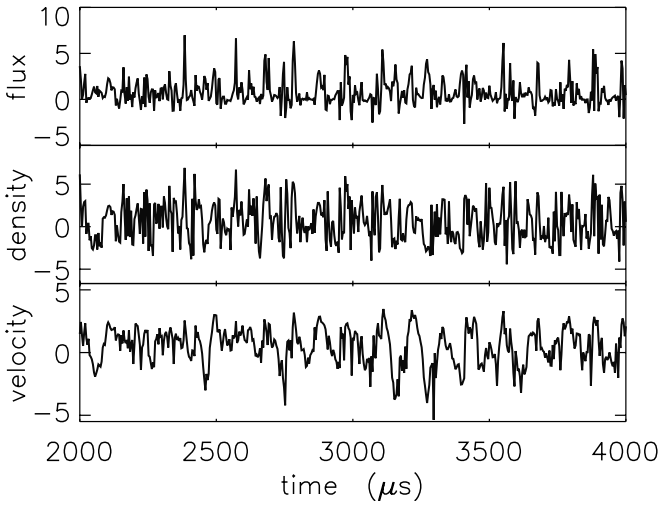

Figure 5. Samples of raw data for the $\Gamma_x = \tilde{n}\tilde{E}_y/B$ component of the fluctuating plasma flux (top frame), the fluctuating density $\tilde{n}$ (middle frame), and the velocity derived from the $\tilde{E}_y$ electric field component (bottom frame). Vertical axes are in units of the RMS values of the corresponding signals.

In figure 5 we show samples of raw data for the fluctuating density $\tilde{n}$, the electric field component $\tilde{E}_y$ and the x-component of the plasma flux $\Gamma_x = \tilde{n}\tilde{E}_y/B$. The velocity (i.e. $\tilde{E}_y$) contains clear bursts of harmonic oscillations, which are here visible in the interval 3000–3500 μs. At other times the burst can have a longer duration. These bursts are not easily visible in the density signal, but are revealed by a correlation analysis. The density signal appears to contain a 'spiky' high-frequency component that is not readily visible in the $\tilde{E}_y$-signal.

The bulk rotation of the plasma column illustrated in figure 3 gives a high Doppler frequency for small scales. We argue that the filtering of small spatial scales by (1) corresponds to a filtering of high frequencies in the signal for $\tilde{E}_y$. Using the bulk plasma rotation velocity at the position $x = 50$ mm, we estimate that frequencies comparable to or larger than 200 kHz are affected by the filtering of the $\tilde{E}_y$-signal due to finite probe separations in (1). The data are acquired with a bandwidth limitation of 125 kHz, so the spatial filtering described by (1) has negligible consequences for our results. Future studies, with higher temporal resolutions, will have to take the spatial filtering into account.

In figure 6 we show the estimates for the amplitude probability density of the fluctuating density, plasma flux and the fluctuating electric field component $\tilde{E}_y$ as obtained at the reference position $x = 50$ mm for the present conditions. At this position we find a negative electric field skewness, $S \equiv \langle(\tilde{E}_y - \langle\tilde{E}_y\rangle)^3\rangle/\sigma^3 \approx -0.85$, where σ is the standard deviation. The signal is leptokurtic by having a positive kurtosis as compared with the reference value for Gaussian signals, $K \equiv \langle(\tilde{E}_y - \langle\tilde{E}_y\rangle)^4\rangle/\sigma^4 - 3 \approx 1.56$. Figure 6 also

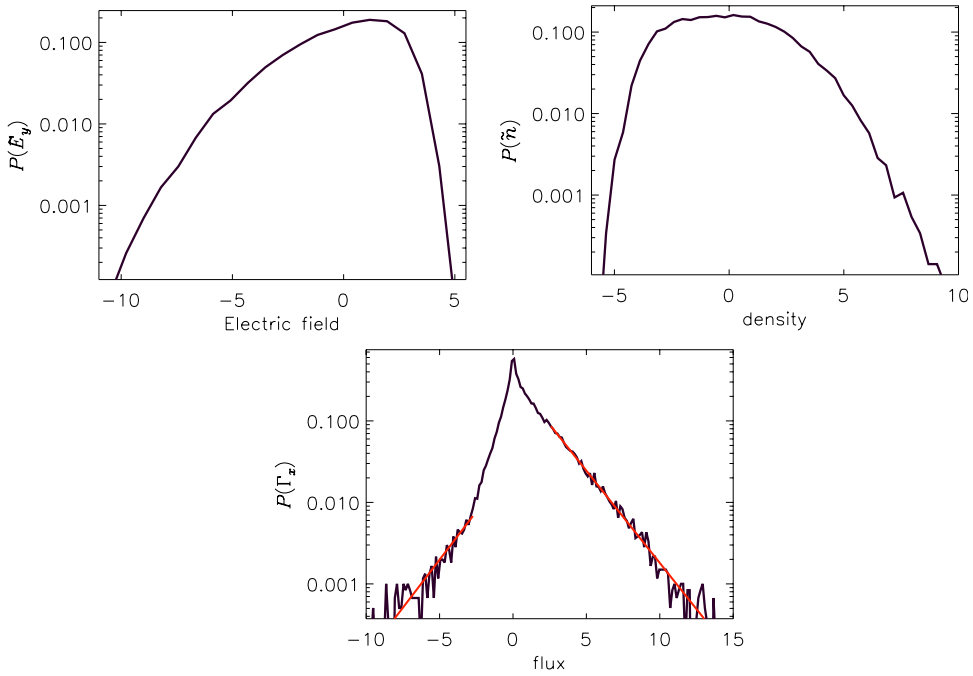

Figure 6. Amplitude probability density of the fluctuating velocity component $\widetilde{E}_y/B$ (top left) and the fluctuating density $\widetilde{n}$ (top right) as detected at the reference position, $x = +50$ mm. Positive values of $\widetilde{E}_y$ imply here an $\boldsymbol{E} \times \boldsymbol{B}/B^2$-velocity out of the plasma column. The probability density of the radial component of the turbulent flux $\Gamma_x = \widetilde{n}\widetilde{E}_y/B$ is obtained at the same position (bottom). All horizontal axes are in RMS units. Red lines indicate exponential fits. Note logarithmic vertical axes on all figures.

contains the probability densities for the fluctuating density and the plasma flux at the same spatial position. Note here that Γ_x contain a component that does not vanish upon averaging. For large values of Γ_x the probability density $P(\Gamma_x)$ can be well approximated by an exponential, while $P(\widetilde{n})$ and $P(\widetilde{E}_y)$ are closer to Gaussians for large values of the respective arguments. In the following we will express results in terms of RMS signal values: for the relative density variations at the position $x = 50$ mm we have $\sqrt{\langle(\widetilde{n}/\overline{n})^2\rangle} \approx 0.22$ while the potential difference between the two probes estimating the $\widetilde{E}_y$ electric field component has an RMS value of 0.58 V, implying an RMS value of the $\widetilde{E}_y/B$-velocity being approximately 570 m s^{-1}, i.e. a value much smaller than the sound speed.

Using data from the position $x = 50$ mm, we show in figure 7 the experimental estimates for the normalized auto-correlations $\langle\widetilde{n}(t)\widetilde{n}(t+\tau)\rangle/\langle\widetilde{n}^2\rangle$ and $\langle\widetilde{E}_y(t)\widetilde{E}_y(t+\tau)\rangle/\langle\widetilde{E}_y^2\rangle$. Similarly we show also the auto-correlation function of the x-component of the fluctuating plasma flux. All auto-correlation functions have 'cusps' at the origin, indicating that the signals are characterized by large values of the time derivatives, i.e. $\langle(\mathrm{d}\widetilde{n}(t)/\mathrm{d}t)^2\rangle$ is large, and similarly for the other signals. While $\widetilde{E}_y$ and $\widetilde{n}$ contain a clear harmonic component, this is less visible in the auto-correlation for the flux. The last curve in figure 7 is the cross-correlation of fluctuating density $\widetilde{n}$ and the fluctuating electric field component $\widetilde{E}_y$ given as $\langle\widetilde{n}(t)\widetilde{E}_y(t+\tau)\rangle \Big/ \sqrt{\langle\widetilde{n}^2\rangle\langle\widetilde{E}_y^2\rangle}$. The auto-correlations are symmetric by construction, but the cross-correlation could be expected to be asymmetric: this turns out not to be the case. Only small signs of asymmetry are found. These features are recovered also when analysing data for $x = -40$ mm. The symmetry of the cross-correlation indicates that there are no significant phase

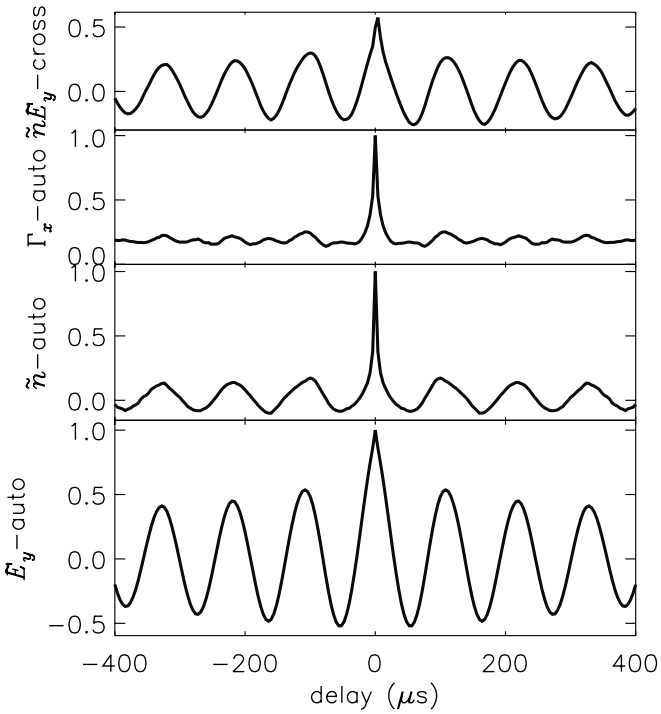

Figure 7. The top frame shows the normalized cross-correlation between the fluctuations in $\widetilde{n}$ and $\widetilde{E}_y$. The next frame gives the auto-correlation for the plasma flux as given by $\widetilde{n}\widetilde{E}_y/B$, where we note the dc level. The third frame from the top shows the auto-correlation for the fluctuating density $\widetilde{n}$. The normalized auto-correlation of the fluctuating electric field component $\widetilde{E}_y$ is shown in the bottom frame as a function of time delay. The data refer to the position $x = 50$ mm.

shifts between the correlated parts of the fluctuating density $\widetilde{n}$ and $\widetilde{E}_y$. At other spatial positions (larger x values) we can observe a phase shift. The normalized cross-correlation at $\tau = 0$ is approximately 0.5, indicating that a model for the fluctuating quantities can contain two components: one with weakly coupled density and $\widetilde{E}_y$ components, and a bursty part where $\widetilde{n}$ and $\widetilde{E}_y$ are strongly coupled. Related results were found also in other experiments [1] and we find the similarity between these two data-sets interesting, in particular because they were obtained in completely different devices.

The general nature of the fluctuations dominating the turbulent transport has been discussed in other studies: flute modes being one limiting case where it can be argued that $k_\parallel = 0$, while for drift-wave type fluctuations it is generally expected that $k_\parallel \neq 0$. The distinction is in reality somewhat artificial, since the flute mode represents a limiting case for a general linear dispersion relation which includes also drift waves. Determining the magnitude of the $\boldsymbol{B}$-parallel wavelength is nonetheless relevant. For a linear device, a Q-machine in particular, the sheath conditions are important for limiting $\lambda_\parallel$ [39]. For a Q-machine plasma with length L, bounded by two warm sheaths (two hot plates), it can thus be argued that $\lambda_\parallel = 2L$, at most. For the scrape-off layer where some early Q-machine studies were carried out [1, 2, 5], the sheath conditions were not well defined, and the question of $\lambda_\parallel$ could not be resolved; all that could be shown was that it was a long wavelength. In a toroidal plasma as the present one it could be explicitly demonstrated [12] that the large coherent structures that dominate the turbulent transport had no associated phase shift in the toroidal direction. The electrostatic modes studied here are flute type.

4. Turbulent fluxes

The fluctuating plasma flux is here identified by $\boldsymbol{\Gamma} = n\boldsymbol{E} \times \boldsymbol{B}/B^2$. We assume quasi-neutrality, $n_e \approx n_i \equiv n$. For steady-state conditions we have $\overline{n} \equiv n_0(\boldsymbol{r})$ and $\overline{\boldsymbol{E}} \equiv \boldsymbol{E}_0(\boldsymbol{r})$, where an overline indicates time averages. We have, for instance, $\langle n_0 \boldsymbol{E} \times \boldsymbol{B}/B^2 \rangle = 0$ while $\boldsymbol{\Gamma}_0 \equiv \langle n\boldsymbol{E} \times \boldsymbol{B}/B^2 \rangle \neq 0$. In the following we will analyze the statistical properties of the radial component of the fluctuating $n\boldsymbol{E} \times \boldsymbol{B}/B^2$ vector, denoted Γ_x. By this we omit components that vanish upon averaging.

The space-time varying signal $\Gamma_x(x, t)$ is obtained at selected positions with 10 mm separation along a line passing through the center of the plasma column. The amplitude probability density for Γ_x is shown in figure 6. The most probable fluxes are small, but the average is significant and positive for $x > 0$. The plasma geometry and methods of plasma production in the present device are completely different from, for instance, the Q-machine where turbulent flux probability densities were first obtained [1]. Nonetheless, we note a surprising similarity between probability density $P(\Gamma_x)$ found here and those obtained in other similar devices [1, 5, 40].

The details of the data-sets vary with radial position in the plasma and consequently also the flux probability density $P(\Gamma_x)$ changes with x. We analyzed the lowest order moments $\langle \Gamma_x^m \rangle \equiv \int_0^\infty \Gamma_x^m P(\Gamma_x) \mathrm{d}\Gamma_x$, for $m = 1, 2, 3, 4$, see also figure 8

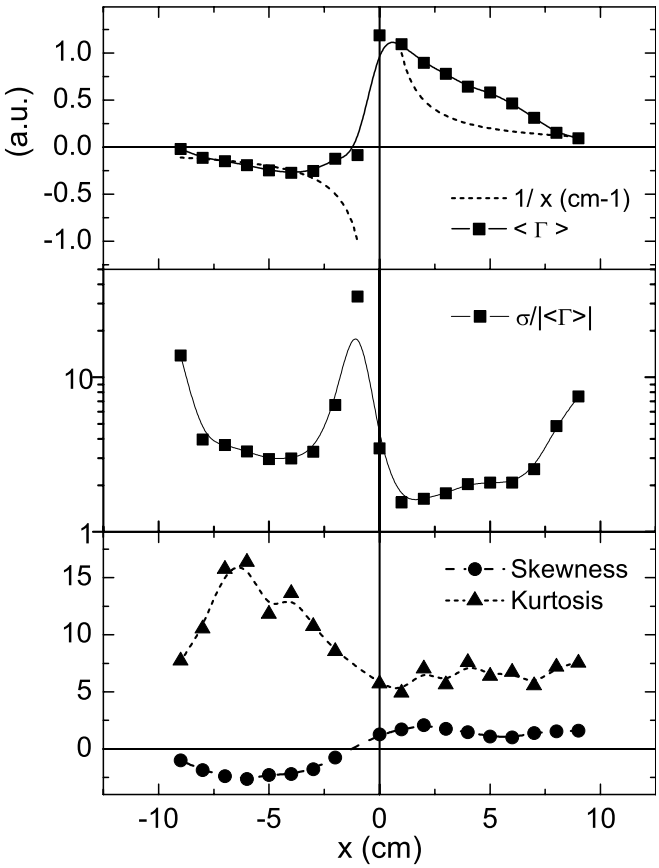

Figure 8. Variation (in arbitrary units) of the average flux $\langle \Gamma_x \rangle$ with position (top frame). Similar variations of its normalized variance $\sigma/|\langle \Gamma_x \rangle| \equiv \sqrt{\langle \Gamma_x^2 \rangle - \langle \Gamma_x \rangle^2}/|\langle \Gamma_x \rangle|$, skewness $\langle (\Gamma_x - \langle \Gamma_x \rangle)^3 \rangle/\sigma^3$ and kurtosis $\langle (\Gamma_x - \langle \Gamma_x \rangle)^4 \rangle/\sigma^4 - 3$ (bottom frame). The position $x = 0$ corresponds to the center of the circular cross-section of the vessel. Two curves $1/x$ and $-1/x$ are inserted with dashed lines for reference in the presentations of the radial variation of the average flux. Note the logarithmic vertical scale for $\sigma/|\langle \Gamma_x \rangle|$.

for a summary. The variation of the average flux $\langle \Gamma_x(x) \rangle$ is particularly interesting. We find $\langle \Gamma_x \rangle > 0$ for $x > 0$ and $\langle \Gamma_x \rangle < 0$ for $x < 0$ implying that the average turbulent flux is directed out of the plasma column in both cases, while the numerical magnitude of the flux is largest for $x > 0$. The change in sign of $\langle \Gamma_x(x) \rangle$ at $x = 0$ has a corresponding change in sign of the skewness, see figure 8. The experimental record lengths are marginally sufficient for estimating the kurtosis, which is consequently somewhat more irregular than the variance and skewness. It is not advisable here to make estimates of fifth or higher order averages. For $|x| < 7$ cm, the error in the kurtosis is typically 20%, while it is 10% or less on the skewness, standard deviations, and the average fluxes. The error is somewhat larger for the last two spatial positions, where the average plasma density is low.

Even when the turbulent flux has an azimuthal variation as in the present case, we would expect that $\langle \Gamma_x \rangle \sim 1/x$. We can test this dependence by our flux measurements along the x-axis. For comparison we inserted reference lines for $1/x$ in the figure for $\langle \Gamma_x(x) \rangle$. For $x < 0$ we find a possible agreement with this $1/x$-variation, but the fit clearly fails for $x > 0$. We expect this to be a sign of an additional loss channel, most likely

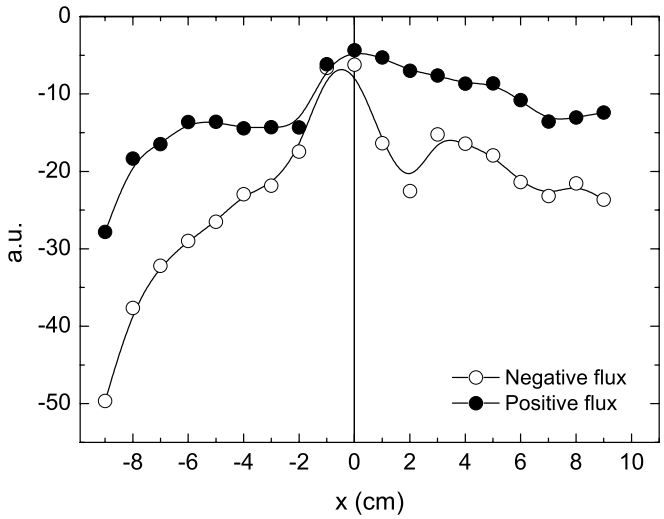

Figure 9. Results from an exponential fit $\exp(-\beta|\Gamma_x|)$ to the PDF for the turbulent flux. We show the variation of the exponent β with x position. The scatter in data points indicates the uncertainties resulting from different choices of Γ_x-intervals for the fit. Solid lines indicate a fit to the experimental points.

to be found in the weak externally imposed vertical magnetic field. We note that the collisions with neutrals give rise to classical diffusion, which is not observed by the diagnostics used in this study.

To obtain some additional information on details in $P(\Gamma_x)$ we made two types of analysis: (i) making a power-law fit $\Gamma_x^{-\alpha}$ for large positive as well as negative values of Γ_x and analyzing the variation of the exponent α with x and (ii) fitting an exponential $\sim\exp(-\beta\,|\Gamma_x|)$, also for large positive as well as negative values of Γ_x and analyzing the variation of the coefficient β with x. See figure 6 for an example.

The first analysis (i) gave only inconclusive results. A power-law fit was indeed possible but only for a limited range for the largest Γ_x-counts in the PDF. The uncertainty became too large for the results to be of relevance here. Still we find it an interesting possibility: if it turns out that the probability density for the fluctuating plasma flux has an asymptotic variation like $\sim\Gamma_x^{-\alpha}$, this will imply that an average like $\langle\Gamma_x^{\alpha-1}\rangle$ is diverging. Results from analysis (ii) were more conclusive and some of the results for the x-variation of the fitted β values are summarized in figure 9. We show β in arbitrary units since there is no natural or absolute normalizing Γ_x value available: the relevant normalization would be Γ_0, but this quantity is varying with x positions, and will not serve for an absolute normalization. We note that we have a systematic variation of $\beta(x)$, indicating that the exponential fit $\exp(-\beta\,|\Gamma_x|)$ is not sporadic. The fit is obtained both for the part of the PDF that represents flux into (open circles) and out of the plasma (filled circles). The large flux limits of both parts of the PDF seems well approximated by an exponential fit, but the two corresponding β values are noticeably different, except near $x = 0$, where the PDF is close to be symmetric with $\langle\Gamma_x\rangle \approx 0$. We note that neither β nor any of the flux moments $\langle\Gamma_x^n\rangle$, with $n = 1, 2, 3, 4$ have abrupt changes near the positions $x = \pm 40$ mm, where the rotation velocity has a significant shear, see also figure 3. This observation indicates that the Kelvin–Helmholtz instability does not have any significant role in the formation of the turbulent spectrum.

5. Intermittency

The word 'intermittency' is often used in descriptions of classical incompressible turbulent flows to account for the inhomogeneous nature of energy dissipation, or inhomogeneity in the distribution of other scalar quantities. The problem with such a vague definition is that *any* random process will exhibit inhomogeneities, also Gaussian processes. This leads to a definition adopted by some authors [41] that 'any variable with zero mean will be called intermittent if it has a probability distribution such that extremely small and extremely large excursions are more likely than in a normally distributed variable'. In this sense, a random Gaussian process serves as the reference for a non-intermittent case. Classical studies of intermittency effects are based on higher order structure functions [42]. These have been applied for studies of plasma turbulence as well. In this study we will use a different approach.

For low-frequency electrostatic field-aligned fluctuations in magnetized plasmas evidence has been found for large intermittent coherent structures being an important constituent of the turbulence. These structures have an important role in the turbulent transport [5, 21, 22] as studied also in the present work. The dynamics of the structures are influenced by the average shear in the plasma flow across magnetic field lines [5, 43, 44]. These structures have previously been identified by conditional sampling techniques [10] also in the present Blaamann device [7, 15].

In order to analyze the intermittent features of the flux signal we suggest here the use of excess statistics, i.e. a study of the duration of time intervals where the flux exceeds some prescribed threshold level. We believe this definition to be particularly useful for studies of confinement of hot plasmas: it can here be important to distinguish many short plasma bursts from a few long ones. Although the accumulated time in the bursts can be the same, their consequences will be different as far as, for instance, the heat load on a confining wall is concerned. With many short bursts there can be time for the wall to cool down between bursts, while it need not be so for a long burst even when they are few. We therefore consider the flux signal obtained from the experiment and analyze the distribution of the time intervals spent above some prescribed reference level. The full analysis involves the probability density of the time intervals $\Delta\tau$, where the signal exceeds some given threshold A, implying that this PDF is conditional, $P(\Delta\tau|A)$, depending on the selected threshold level. Experimentally, the analysis is feasible, and in figure 10 we show sample results of estimates for probability densities $P(\Delta\tau|A)$. We note that as the threshold level A increases, the probability for short $\Delta\tau$ is decreasing, while the probability for finding large $\Delta\tau$ is reduced only little in comparison. For all levels A we find that the most probable time interval lengths are short, but $P(\Delta\tau|A)$ has a long tail of up to $40 - 50\,\mu$s duration.

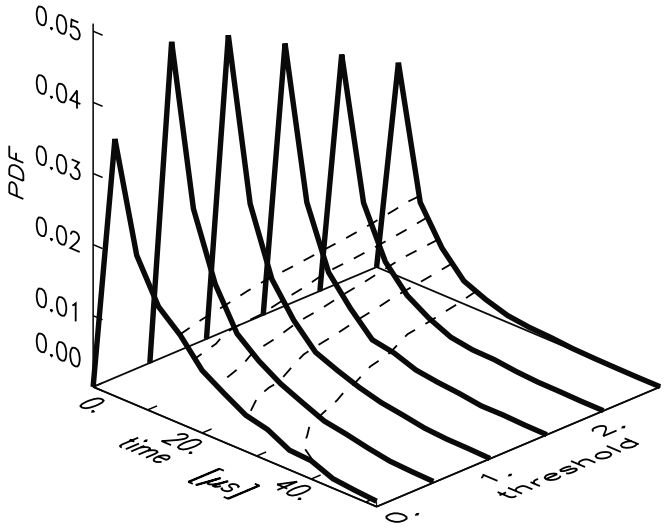

Figure 10. Experimentally obtained estimates for probability densities $P(\Delta\tau|A)$ of the time intervals $\Delta\tau$, where the signal exceeds a given threshold A, for six selected threshold levels. Threshold levels are given in units of the RMS value of the flux signal. The distribution is here normalized over the plane shown. A few contour levels for constant probability density are shown by dashed lines.

For practical purposes, the probability density $P(\Delta\tau|A)$ will contain too much information. It is an advantage to reduce the analysis to deal with its average value as illustrated in the following section.

We postulate that the rate of level crossings and the average duration of excess times offer very sensitive indicators of intermittent features in a signal. In order to obtain a basis for comparison, we need an expression for the result that would be obtained for the equivalent Gaussian signal: equivalent in the sense that is has the same average and standard deviation. Such an expression can be determined by the joint probability density of the flux signal and its time derivative [45–48].

5.1. Average number of level crossings

A complete discussion of the statistical distribution of excursions in a random signal (such as the velocity or the electric field magnitude) is complicated. Analytical expressions for the duration of times spent by such a signal at amplitudes exceeding some selected levels can be found in the literature [46], but the practical applicability of these results is restricted to short times. Some useful estimates can, however, be obtained by simpler means [45, 48]. We assume the amplitude probability density $P(\Gamma_x)$ to be given. Since there can be a net flux, there are no restrictions on the average values, implying that $\langle\Gamma_x\rangle \neq 0$ in general. Given a long time interval of duration $\mathcal{T}$, the time spent above a given reference level A is then $\Theta(A) = \mathcal{T}\int_A^\infty P(\Gamma_x)\mathrm{d}\Gamma_x$. This time interval can be obtained in many different ways, i.e. by many short excursions above A or alternatively just a few, but long ones, for instance. To find the average number of excursion in the interval $\mathcal{T}$ we need to know also the distribution of the time derivative $\mathrm{d}\Gamma_x(t)/\mathrm{d}t \equiv \Gamma'_x$ of the signal [46, 49], i.e. the joint probability density $P(\Gamma_x, \Gamma'_x)$. The assumed time-stationarity of the process becomes essential here by implying that $P(\Gamma_x, \Gamma'_x)$ is independent of time.

The ensuing analysis consists of two steps, where details are found elsewhere [45, 46, 48]. First we note that the time it takes for the signal to cross a small interval $\mathrm{d}\Gamma_x$ is given as $\mathrm{d}\Gamma_x/\Gamma'_x$. We then note that $P(\Gamma_x, \Gamma'_x)\mathrm{d}\Gamma_x\,\mathrm{d}\Gamma'_x\mathrm{d}t$ is the average fraction of time spent by the signal in an interval $\mathrm{d}t$ around any set of amplitudes and time derivatives $\{\Gamma_x, \Gamma'_x\}$ within a narrow interval $\mathrm{d}\Gamma_x\mathrm{d}\,\Gamma'_x$. The average number $\mathcal{N}$ of upward crossings of the level $\Gamma_x = A$ in the time interval $\mathcal{T}$ is then obtained by two integrations. First an integration with respect to time over the interval $\{0, \mathcal{T}\}$, which becomes simple since $P(\Gamma_x, \Gamma'_x)$ is independent of time, and then an integration with respect to all positive values of Γ'_x, implying that we include all upward crossing irrespective of the numerical value of Γ'_x. The result of these two integrations is

$$\mathcal{N}(A) = \mathcal{T}\int_0^\infty \Gamma'_x P(A, \Gamma'_x)\mathrm{d}\Gamma'_x. \tag{3}$$

As the next step, an estimate for the time spent in excess of a selected signal level $\Gamma_x = A$ is then found by dividing the total time spent with $\Gamma_x \geqslant A$ with the average number of upward crossings [45]. This gives

$$\frac{\Theta(A)}{\mathcal{N}(A)} = \frac{\int_A^\infty P(\Gamma_x)\mathrm{d}\Gamma_x}{\int_0^\infty \Gamma'_x P(A, \Gamma'_x)\mathrm{d}\Gamma'_x}, \tag{4}$$

independent of $\mathcal{T}$. In the limit of $A \to -\infty$ we find $\Theta(A)/\mathcal{N}(A) \to \infty$ since we have $P(A \to -\infty, \Gamma'_x) \to 0$. For $A \to -\infty$ the entire (infinitely long) record will exceed the reference level. Our working hypothesis [45] is that the result (4) is approximating $\int_0^\infty \Delta\tau P(\Delta\tau|A)d\Delta\tau$: it is thus not an exact result since it is obtained by taking the ratio of two averages, where a full analysis would be based on the conditional probability distribution of the excess time intervals $P(\Delta\tau|A)$.

In general we have no a priory knowledge of $P(\Gamma_x, \Gamma'_x)$, except from the fact that Γ_x and Γ'_x are uncorrelated, since $\langle(\Gamma_x(t) - \langle\Gamma_x\rangle)\mathrm{d}\Gamma_x/\mathrm{d}t\rangle = \frac{1}{2}\mathrm{d}\langle\Gamma_x(t)^2\rangle/\mathrm{d}t = 0$, with $\langle\Gamma'_x\rangle = 0$ and $\langle\Gamma_x(t)^2\rangle$ being a constant for time stationary conditions. It is, however, possible to obtain an estimate of $P(\Gamma_x, \Gamma'_x)$ experimentally, see, figure 11. The flux is given in arbitrary units from the experiment, and its time derivative is approximated by $\Gamma'_k \approx (\Gamma_{k+1} - \Gamma_{k-1})/2\Delta t$, where k is the time sample number. We show $P(\Gamma_x, \Gamma'_x)$ for two positions, $x = -40$ mm and $x = +50$ mm. The center of each of the two figures is placed at the average value $\{\langle\Gamma_x\rangle, \langle\Gamma'_x\rangle\}$. Ideally we would have $\langle\Gamma'_x\rangle = 0$, but due to finite record lengths we have small deviations from the ideal case. For both examples shown in figure 11 we find that $P(\Gamma_x, \Gamma'_x) \neq P(\Gamma_x)P(\Gamma'_x)$, and the flux process can not be approximated by a Gaussian random process.

5.2. The Gaussian limit

The Gaussian non-intermittent reference model can be analyzed by the previously obtained analytical expressions

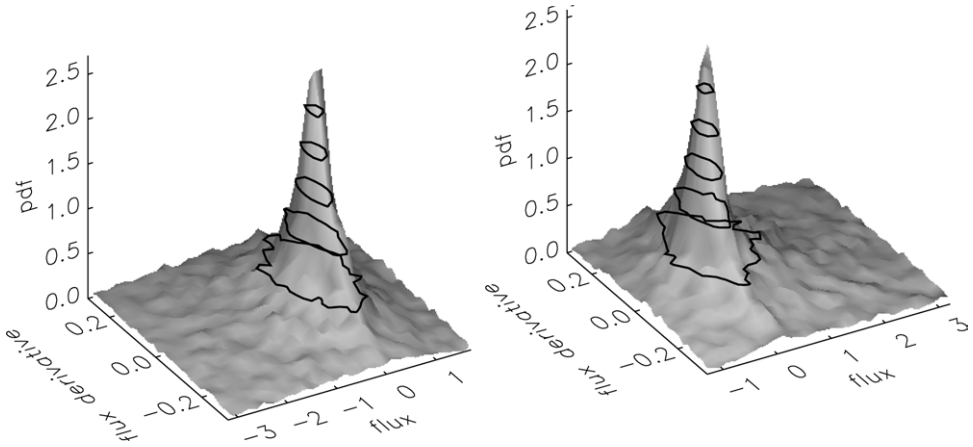

Figure 11. Experimentally obtained estimates of the joint probability density $P(\Gamma_x, \Gamma'_x)$ for two positions: left at $x = -40$ mm (with average flux in the negative x-direction) and right at $x = 50$ mm (with average flux in the positive x-direction). Note the differences in intervals on the axes.

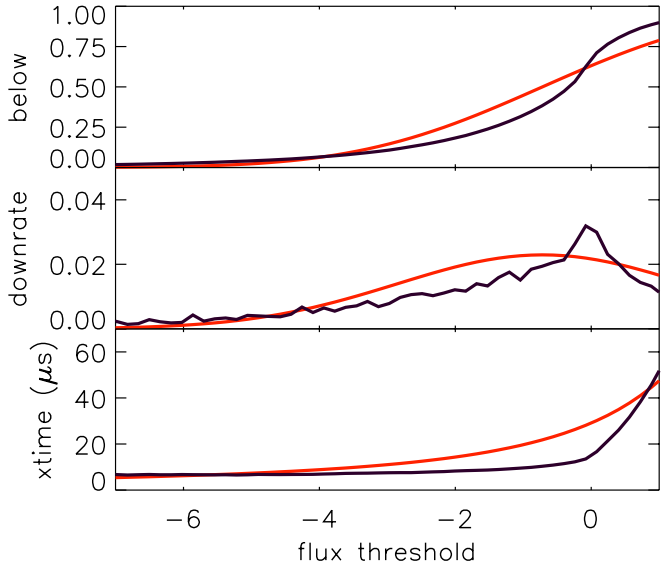

Figure 12. Top: fraction of time in the flux signal spent below threshold levels. Middle: rate of the threshold crossings of the flux signal. Bottom: average length of time intervals (denoted 'xtime' for 'excess time') spent below the threshold levels. Red lines give in all cases the analytical results for a Gaussian reference model having the same average and standard deviations as the flux signal. Flux thresholds are given in RMS values of the flux signal. $x = -40$ mm.

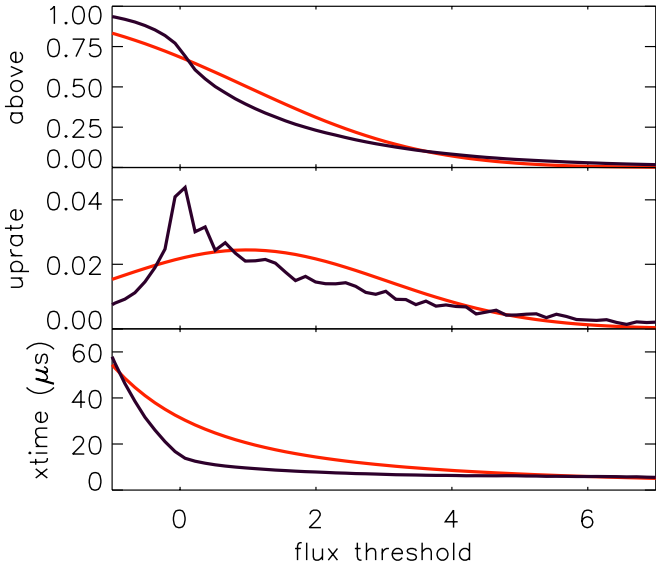

Figure 13. Top: fraction of time spent above threshold level, shown for varying levels. Middle: rate of the threshold crossings of the flux signal. Bottom: average length of time intervals spent above threshold levels. The figure set-up is the same as described in figure 12. Flux thresholds are given in RMS values of the flux signal. $x = 50$ mm.

[45, 48]. Being uncorrelated, the flux signal Γ_x and its time derivative Γ'_x are also statistically independent in the Gaussian limit. We can then write the joint probability density as a product $P(\Gamma_x, \Gamma'_x) = P(\Gamma_x)P(\Gamma'_x)$, where the two probability densities are characterized by their averages $\langle\Gamma_x\rangle$ and $\langle\Gamma'_x\rangle = 0$, together with their standard deviations σ^2 and σ'^2. These are related by the power spectrum $G(\omega)$ of $\Gamma_x(t)$: we have $\sigma^2 = \int_0^\infty G(\omega)\mathrm{d}\omega$ and $\sigma'^2 = \int_0^\infty \omega^2 G(\omega)\mathrm{d}\omega$ for stationary random processes. We can define an average mean square frequency as $\langle\omega^2\rangle \equiv \int_0^\infty \omega^2 G(\omega)\mathrm{d}\omega \Big/ \int_0^\infty G(\omega)\mathrm{d}\omega$, in which case we have the simple physical interpretation $\sigma/\sigma' = 1\Big/\sqrt{\langle\omega^2\rangle}$.

In the 'non-intermittent Gaussian limit' we find after some calculations the relatively simple result

$$\frac{\Theta(A)}{\mathcal{N}(A)} = \pi\frac{\sigma}{\sigma'}\exp\left(\frac{1}{2}(A - \langle\Gamma_x\rangle)^2/\sigma^2\right) \times \mathrm{erfc}\left(\frac{1}{\sqrt{2}}(A - \langle\Gamma_x\rangle)/\sigma\right). \quad (5)$$

where $\mathrm{erfc}(x) \equiv (2/\sqrt{\pi})\int_x^\infty \exp(-\xi^2)d\xi$ is the complementary error function. For $A \to -\infty$ we find also here that $\Theta(A)/\mathcal{N} \to \infty$.

The results outlined here have been tested by synthetic data [48], in particular to study the transition from non-Gaussian to Gaussian random signals. These studies demonstrate that the rate of level crossings and the average duration of excess times

offer very sensitive indicators for deviations from Gaussian properties of a given signal.

The analysis of the statistical scatter of the excess times requires in part also knowledge of the expected value of the number of level crossings in a time interval dt_1 through $(\Gamma_1, \Gamma_1 + d\Gamma_1)$ with derivative Γ_1', multiplied with the number of level crossings in a time interval dt_2 through $(\Gamma_2, \Gamma_2 + d\Gamma_2)$ with derivative Γ_2'. One is led to consider the fourth-order joint probability density $P_{t_1,t_2}(\Gamma_{x1}, \Gamma_{x1}', \Gamma_{x2}, \Gamma_{x2}')$. The analysis is simple only for Gaussian random signals [49], and this study is outside the scope of this work.

5.3. Experimental results for average times for level crossings

Given the experimental records, we analyze the data to obtain the basic information of the level crossing distributions. Results are shown here for two positions $x = -40$ mm and $x = 50$ mm, see also figure 11. In figure 12 we show results for $x = -40$ mm where the average flux is in the negative x-direction. The top frame shows the fraction of time the flux signal spent below negative threshold levels shown as a function of the threshold level. The middle frame shows the rate of the threshold crossings of the flux signal. The bottom frame shows the average length of time intervals spent below the threshold levels. In figure 13 we show similar results for $x = 50$ mm where the average flux is in the positive x-direction. In both figures 12 and 13 we have a red line giving the results for an equivalent Gaussian random process. By interpolation we obtain a time resolution that is better than the inverse sampling rate.

We find significant non-Gaussian features in the flux signal, demonstrating that the excess time statistics is a good indicator for intermittent features. In particular we note that the average excess times (bottom curves in figures 12 and 13) show a long interval where this average time is only slowly reducing for increasing threshold levels. Long time durations are rare for fluxes exceeding low threshold values when compared with Gaussian processes. In, for instance, figure 13 we can extend the flux-threshold axis to 8 and still observe some very short time intervals, until at even larger threshold values the number of events reach zero when the imposed threshold level exceeds the maximum flux value of the given records.

We see that large amplitude bursts are rare, i.e. the number of level crossings reduce rapidly with increasing threshold, although they are slightly more frequent than for the equivalent Gaussian random process. The average duration of the bursts is, however, only slightly smaller than for smaller threshold levels. The number of very large amplitude bursts is thus small, but individually they carry an amount of plasma material that is large compared with the equivalent Gaussian random process.

A conclusion consistent with the observations in figures 12 and 13 is that the flux signal has a low level of random fluctuations, where inwards and outwards plasma flux is of equal probability. In addition to this we have sporadic bursts of plasma, where the flux is rapidly increasing to reach a high level and then rapidly decreasing with a burst duration of typically 10^{-5} s. These bursts propagate, on average, plasma out of the plasma column. For small thresholds, the average width of the bursts is small and they are more rare as compared with the equivalent Gaussian random process. As the threshold increases, the width reduces slowly and also the frequency of occurrence reduces. A Gaussian process would, in comparison, have a faster decline with increasing threshold.

The basic characteristics of the lowest order averages of the plasma flux probability density change noticeable for $x < 0$ to $x > 0$, see figure 8. The temporal intermittency characteristics as evidenced by the excess statistics is more robust, being approximately the same for $x < 0$ and $x > 0$, see figures 12 and 13.

The largest uncertainties in figures 12 and 13 are found for the rates of level crossings (found in the middle panels), where we estimate the uncertainties to be $\pm 15\%$. The peak deviation between the equivalent Gaussian signal is, however, close to 80%, so our conclusion is robust also for this most uncertain case. At other flux threshold levels the differences can be smaller, but the variation is systematic and consistent with non-Gaussian features. The construction of the curves for the equivalent Gaussian signal does not introduce additional uncertainties since it is based on the average and variance of the original data-set. Also we note that the variations in figures 12 and 13 are consistent, although the results refer to opposite positions in the plasma torus.

The results in figures 12 and 13 give indications of frequencies of occurrences and average widths of the structures, but contains no information on details of the temporal variation of the plasma bursts. This information is best obtained by a conditional averaging.

6. Conditional analysis

Detailed information concerning the turbulent fluxes can be obtained by conditional averaging. This method and its generalization have been discussed in the literature [10, 12, 13, 15, 16, 50] and need not be repeated here in detail. For the present study we select upward crossings of a reference amplitude level and determine the time interval until the first downward crossing of this level. The maximum signal value in this interval is found and the origin for this window is subsequently placed at the time for this maximum amplitude. When a conditional time window has been selected, the signal is searched for the next upward crossing of the selected reference amplitude, introducing a time delay in order to avoid overlap of subsequent windows. The signals in the selected intervals are then averaged. This procedure outlined here was originally used in previous studies [12]. Several other methods for conditional averages have been used, but these do not reproduce details in the time variation of the averaged fluxes.

6.1. Basic results

The basic results are shown in figure 14 where we have the conditionally averaged flux signals as described before. We imposed the conditions $\Gamma_x \geqslant 0.5$, 1.0, 1.5, 2.0 and 2.5 in terms of the RMS value of the flux signal. We note that the signal has a narrow spike at the reference time for all conditions shown,

but that some widening of the base of the structure appears for large values of the imposed conditions. The duration at half peak value of the averaged burst is relatively constant, approximately 20 μs, independent of the imposed condition as long as it is positive. The signals are skew in all cases, but this feature is most pronounced for small values of the imposed condition.

Figure 15 illustrates cases where the condition is applied only to the flux signal itself as in figure 14, but here we show also the corresponding conditionally averaged density and electric field component. A large amplitude coherent burst in the plasma flux corresponds to one of the examples in figure 14. At first sight it seems surprising that the conditionally averaged electric field component is negative for the case with $x = 50$ mm. This result can be understood by considering the joint probability densities for $\widetilde{n}$ and $\widetilde{E}_y$ as shown in figure 16. Note the 'triangular' shape of the PDF for $x = 50$ mm. We find that a large value of the outgoing plasma flux can in this case be obtained either by a small negative density perturbation together with a large negative $\widetilde{E}_y$ value, or by having large density perturbation together with a small $\widetilde{E}_y$ value. With the PDF shown in figure 16 for $x = 50$ mm we can not have *both* $\widetilde{n}$ and $\widetilde{E}_y$ large at the same time. With the imposed condition being $\Gamma_x > 0$ we find that the conditional average of $\widetilde{n}$ is positive at the reference time while the corresponding average of $\widetilde{E}_y$ is negative, in spite of the fact that the product of the two quantities is positive in each of the conditional realizations: a somewhat counter intuitive result. For the position $x = -40$ mm the joint PDF is more rounded and the conditional fluxes are as expected, recalling that $\langle\Gamma_x\rangle < 0$ here implies a flux in the direction out of the plasma.

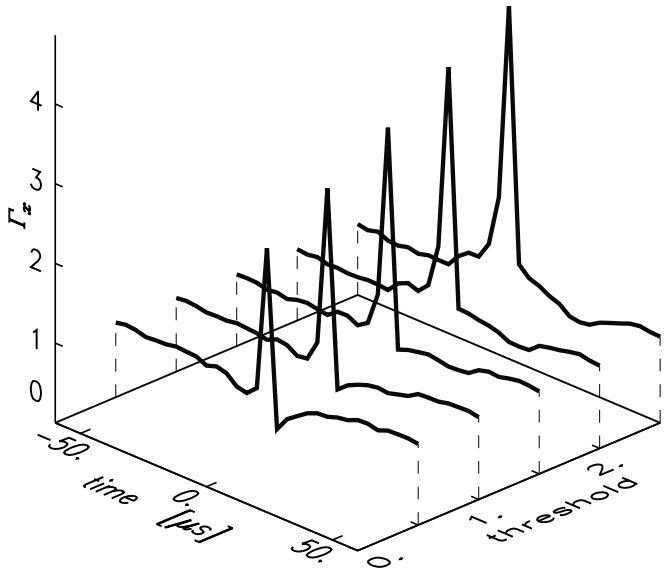

Figure 14. Conditionally averaged flux signals, with imposed conditions $\Gamma_x \geqslant 0.5$, 1.0, 1.5, 2.0 and 2.5 in terms of the RMS value of the flux signal, together with the additional condition $d\Gamma_x/dt > 0$. For large time separations, the conditionally averaged fluxes approach the unconditional average. The position is $x = 50$ mm.

We find that a typical duration of an averaged flux event is $\Delta\tau \sim 15$–$20\,\mu$s. Assuming a characteristic velocity of 2×10^3 m s^{-1} at a position of $x = 50$ mm, see figure 3, we can estimate that this $\Delta\tau$ corresponds to an approximately 3 cm spatial width of the burst in the y-direction. This width is approximately 10 ion Larmor radii.

More generally, we may distinguish contributions to a positive, outgoing flux $\Gamma_x = \widetilde{n}\widetilde{E}_y/B$ for cases where, for instance for $x > 0$ we have $\{\widetilde{n} > 0; \widetilde{E}_y > 0\}$ or $\{\widetilde{n} < 0; \widetilde{E}_y < 0\}$. Both cases give rise to plasma flux out of the plasma column, $\Gamma_x > 0$, but the physical details are different. These cases are discussed in the following.

6.2. *Fluxes for different combinations of $\widetilde{n}$ and $\widetilde{E}_y$*

We have two separate records, one for density $\widetilde{n}(t)$ and one for azimuthal electric field $\widetilde{E}_y(t)$. From this we construct a third record $\Gamma_x(t) = \widetilde{n}(t)\widetilde{E}_y(t)/B$. These three records can be analyzed by imposing conditions or selection rules on combinations of the three signals.

Considering the reference position $x = 50$ mm, we can carry out a conditional analysis with conditions given as $\Gamma_x > 0$ and $\widetilde{E}_y < 0$. An example is shown in figure 17 for the case where the imposed condition is $\Gamma_x > 2$ and $\widetilde{E}_y < -0.5$, both in units of the corresponding standard deviations, without any conditions on $\widetilde{n}$.

A different example is shown in figure 18, where the imposed condition is $\Gamma_x \geqslant 2$ and $\widetilde{n} < 0$, with no conditions on $\widetilde{E}_y$. The interesting observation is here the similarity between figure 17 and the left part of figure 18.

For comparison we also analyzed the case where the imposed condition is $\Gamma_x \geqslant 2$ and $\widetilde{n} > 0$, with no conditions on

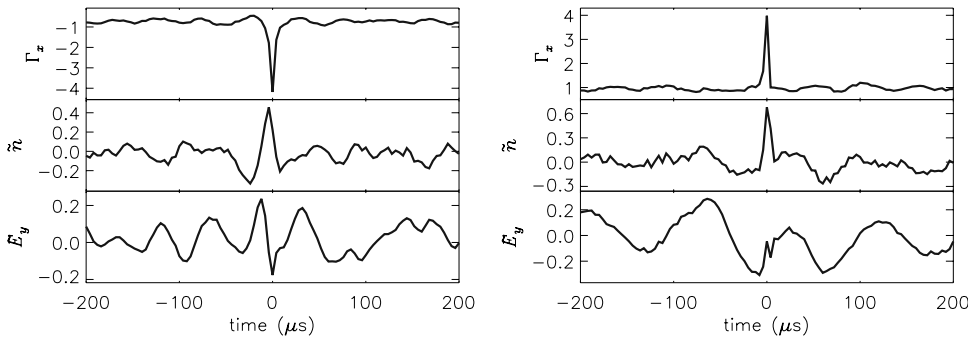

Figure 15. Conditionally averaged fluxes with conditions imposed on the flux signal itself. The left figure is obtained for the position $x = -40$ mm with imposed condition $\Gamma_x < -2$, the one to the right for $x = 50$ mm with imposed condition $\Gamma_x > 2$. No conditions were imposed on $\widetilde{n}$ nor $\widetilde{E}_y$. In both cases shown we have the flux direction out of the plasma column.

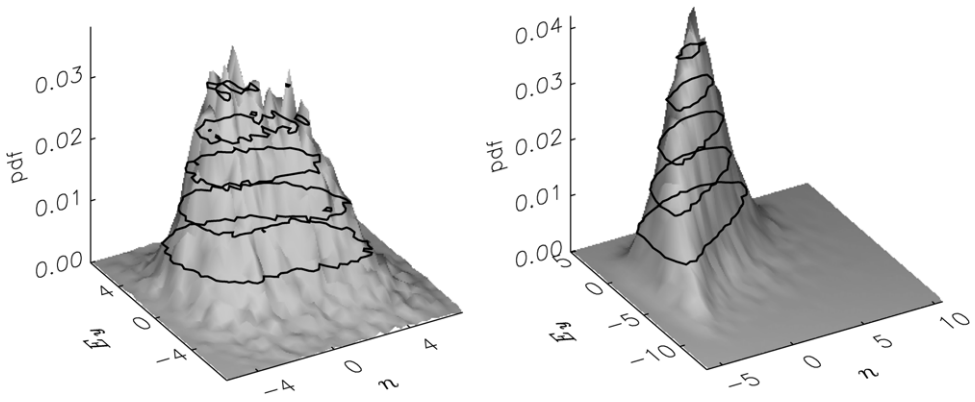

Figure 16. Experimentally obtained estimate of the joint probability density $P(\widetilde{n}, \widetilde{E}_y)$ for two positions: left at $x = -40$ mm and right at $x = 50$ mm.

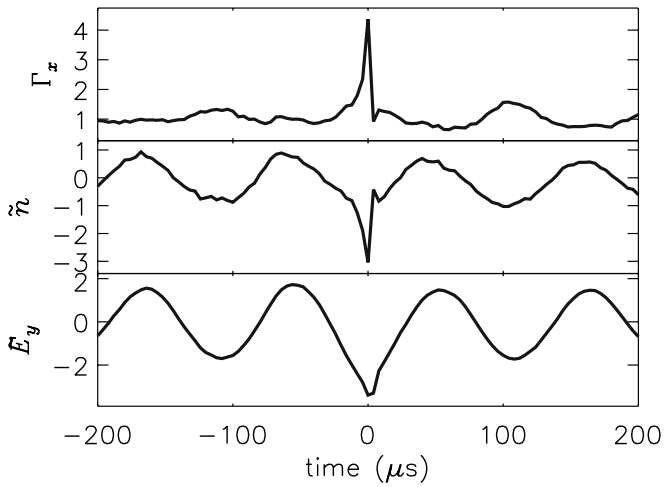

Figure 17. Conditionally averaged signals for the case where the imposed condition is $\Gamma_x \geqslant 2$ and $\widetilde{E}_y < -0.5$, with no conditions on $\widetilde{n}$.

$\widetilde{E}_y$, see figure 18. This case is distinguished from the results in figure 17 by the asymmetry in the conditionally averaged $\widetilde{n}$ and $\widetilde{E}_y$ signals.

As evident from the probability density $P(\Gamma_x)$ there are times where the plasma flux is sporadically inwards, although the average direction is going out of the plasma column. We can gain insight also in the case with $\Gamma_x < 0$ by use of conditional averaging, see figure 15. Studying this case we find only irregular time variations, without pronounced features as found for the outgoing plasma fluxes.

7. Comparisons with other experiments

Conditional averaging was seemingly used first in a linear device [2, 5] for studies of the formation, propagation and decay of large coherent structures. This type of analysis was later used in related studies in many other and different types of magnetized plasma devices [7, 11–13, 15, 16, 23, 51]. Observations of individual structures have been reported as well [17]. Most of these observations mentioned here refer to localized structures, but arguments have been given also for large scale spiral structures that cover a significant part of a plasma cross-section in rotating plasmas [52].

Several studies of turbulent plasma transport due to electrostatic low-frequency magnetic field aligned perturbations show similarities with our results. For illustration we list a few of these in the following.

The PDF of the turbulent flux has been measured in a linear device (Large Mirror Device-Upgrade, LMD-U) and compared also with the momentum flux [40]: this latter analysis seems to be the only one of its sort, for the time being. A related analysis in toroidal devices like Blaamann will be interesting. The form of the PDF for Γ_x found in LMD-U is very similar to ours.

Significant deviations from Gaussian statistics have been reported in devices similar to Blaamann [14] with particular attention to the PDF of the turbulent flux variations, but with limited information on the density and electric field fluctuations. Global measurements (i.e. covering a cross-section of the plasma column), using conditional sampling and averaging [7, 12] demonstrated the existence of large irregular rotating structures, which in a transient time interval could take a dipolar form. A consistent interpretation of the present results taken along a line crossing a section of the plasma is that the smaller irregularities give the low level noise in the flux signal in, for instance, figure 5, while the enhanced local electric field associated with the dipolar structures gives rise to the large localized bursts or spikes also seen in figure 5. This interpretation finds supported in observations [7], although the plasma flux was there estimated by indirect means.

The TORPEX torus is in many ways similar to Blaamann, and coherent localized density perturbations have been observed also in that device by conditional averaging [53, 54]. The results were supported by numerical simulations.

Related studies have been carried out in other types of devices. Studies in the DIII-D tokamak identify two regimes, a high (H) and a low (L) confinement mode, and conditionally averaged flux signals were obtained for both for different radial positions [23]. In particular for the L-mode, the results appear very similar to ours. Both localized enhancements and depletions of the plasma density were identified, and it was found that density depletions propagate mostly inwards, density enhancements out of the plasma.

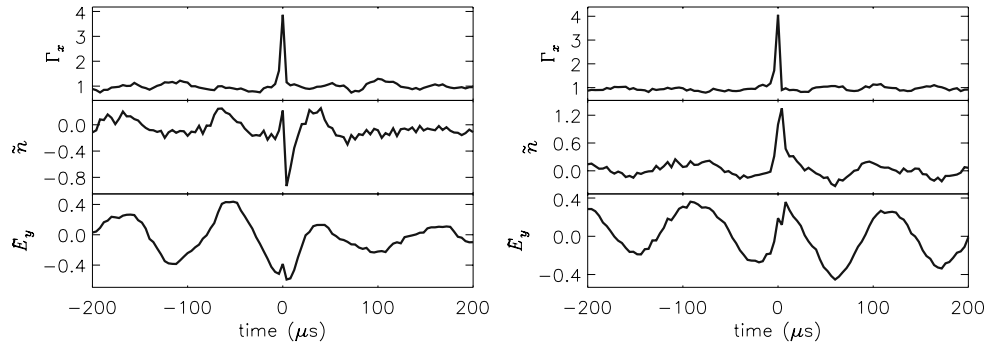

Figure 18. Left: conditionally averaged signals for the case where the imposed condition is $\Gamma_x \geqslant 2$ and $\widetilde{n} < 0$, with no conditions on $\widetilde{E}_y$. Right: conditionally averaged signals for the case where the imposed condition is $\Gamma_x \geqslant 2$ and $\widetilde{n} > 0$, with no conditions on $\widetilde{E}_y$.

Studies of the variations in plasma density in the HL-2A tokamak [51] demonstrate that the conditionally averaged plasma density perturbations (local enhancements as well as depletions) just inside the last closed flux surface appear similar to what we observe here. Density depletions were found to propagate predominantly inwards, density enhancements outwards, thus both cases contributing to a net loss of plasma. The discussion in our section 6.2 contributes with detailed insight to a discussion of the difference between the two processes.

There is no obvious conclusions resulting from the form of the conditional averages. In some, but not all, cases the variations seem to be asymmetric in time. This feature can be found also in our data, but the conclusion will depend on the threshold level used for the condition, see figure 14.

Concerning the use of conditional sampling and averaging it might be appropriate to emphasize some inherent limitations of the method. In particular, the results depend on details in the applied conditions. The original version, as used in studies of plasma turbulence, simply imposed conditions on the signal amplitude and the sign of the time derivative. If the latter constraint was removed, the result changed noticeably, as easily explained by simple model considerations [10]. The conditions used in the present work, as described before, are more restrictive. Some improvements of the method can be obtained, where some studies recommend pre-filtering of the data, with several methods being suggested [15, 50]. Conditional averaging is used mostly because it is simple to implement, and simple to interpret. Other generalizations of the methods, conditional medians for instance, have been suggested [10] but the possible advantages of this procedure remains to be explored.

The relations between the conditionally averaged signal and the individual structures constituting the result can be complicated. Detailed insight can be gained by use of a matched filter [15], where the filter transfer function is chosen according to some a priory information, or presumed knowledge. From figure 14 we can, however, safely conclude that the structures in the flux signal cover a variety of shapes: otherwise the conditionally averaged signals will have the same appearance, irrespective of the imposed condition. The scatter in the pulse shapes with respect to the conditional average is measured by the conditional variance [2, 10]. The statistical spread of the duration of excess times, see figure 10, contains information related to the conditional variance, but this information is not contained in $P(\Gamma_x, \Gamma'_x)$.

It should also be mentioned that conditional sampling and averaging gives some result, irrespective of the nature of the signal, in particular also for a non-intermittent reference Gaussian signal. In that case it is simply the correlation function that is being reproduced. This observation has analytical support [29, 55, 56]. The fluctuations in the TEXT-U tokamak thus seemed to be characterized by near Gaussian statistics [11].

While the basic information of the turbulent transport and the information concerning the excess averages is contained in the flux probability density $P(\Gamma_x)$ and joint probability density $P(\Gamma_x\Gamma'_x)$, it can be demonstrated [29, 55] that the information of the conditional averages is contained in the lowest and higher order auto- and cross-correlation functions. Conditional averages (in the early studies, using some simple conditions, it was denoted 'superposed epoch'), were for a time widely applied in studies of neutral turbulence, with some basic references presented elsewhere [15].

8. Conclusions

We presented results from an experimental study of turbulent transport due to low-frequency electrostatic fluctuations in a magnetized toroidal discharge plasma. We obtained a fluctuating flux signal at selected positions with 10 mm separation along a line crossing the center of the device. In each position we obtained an experimental estimate for the amplitude probability density $P(\Gamma_x)$ for the flux signal Γ_x and studied the spatial variations of the lowest order statistical averages.

Turbulent flux events (or plasma bursts) were studied by conditional sampling methods and it was demonstrated that significant information can be recovered by imposing conditions not only of the flux signal $\Gamma_x \equiv \widetilde{n}\widetilde{E}_y/B$ itself, but also on one or more of its constituent signals, $\widetilde{n}$ or $\widetilde{E}_y$. In particular we can distinguish flux events where $\widetilde{n} > 0$ and $\widetilde{E}_y > 0$ as compared with $\widetilde{n} < 0$ and $\widetilde{E}_y < 0$; both cases give contributions to the flux signal with the same sign, but the time variations of the conditionally averages are very different, see, for instance, figures 17 and 18. Studying the large plasma bursts by a local wavelet transform [15], we

found that in general they appear without any noticeable or significant precursors in the flux signal, but a cross-conditional analysis (where condition is imposed on the flux signal for analyzing $\widetilde{E}_y$ as in the left figure 15) indicates some change in the average frequency of the oscillations before and after the event. Another example is found in the left figure 18, where a change in average oscillation amplitude is found. Even with this generalization of the analysis we fail to observe any precursors of significance for large bursts of plasma.

We found evidence for strong intermittency effects, and demonstrated that statistical distributions of the time intervals spent in excess of some selected flux threshold levels are good indicators for this intermittency. Analytical expressions were presented for some relevant average time intervals, offering in particular results for a Gaussian limit that can be used as a reference non-intermittent case. For the present plasma conditions we found significant deviations from the Gaussian reference model as the threshold was varied. For large thresholds, in particular, we found an excess of the average time interval duration as compared with the reference case. The analysis was based on methods applied for other related problems [45]. The joint probability density $P(\Gamma_x, \Gamma'_x)$ contains all the information needed for an estimate of the average duration of excess time intervals in the sense discussed in section 5.1.

The turbulence in the Blaamann device is characterized by a broad spectrum containing also some narrow spectral components [7]. For the present case the dominant oscillation is shown in the power spectrum (see figure 4) and observable in our auto-correlation measurements as well, as summarized in figure 7. The conditional averaging shown in figures 17 and 18 demonstrates that the bursts and the harmonic oscillations are phase correlated: otherwise the oscillations should disappear by the statistical averaging. A general conclusion for figures like 15, 17 and 18 is that large fluxes, $\Gamma_x > 2$ (in units of the standard deviation), occur for large temporally narrow 'spikes' in the density signal, $\widetilde{n}$, and also rapid variations in $\widetilde{E}_y$.

An interesting result from our analysis is a demonstration of the significant changes in the joint probability densities $P(\widetilde{n}, \widetilde{E}_y)$ observed as the fluctuations propagate from the outer ($x > 0$) low magnetic field side to the inner ($x < 0$) high magnetic field side of the plasma, see figure 16. The observed difference is likely to be caused by the spatial magnetic field variation, which implies that $\nabla\cdot(\nabla\phi \times \boldsymbol{B}/B^2) \neq 0$, in contrast to the result for $B = \text{const.}$, where the $\boldsymbol{E} \times \boldsymbol{B}/B^2 = -\nabla\phi \times \boldsymbol{B}/B^2$-flow is incompressible. This observation applies both for the fluctuating and for the steady-state parts of the electric fields. For the present toroidal conditions, the bulk $\boldsymbol{E}_0 \times \boldsymbol{B}/B^2$-rotation gives rise to a compression of a small reference plasma volume as it moves from a position at $x > 0$ to $x < 0$. In comparison, we find that the turbulent frequency spectra are independent of the azimuthal position and depend only on the radial variable for the constant magnetic fields found in linear Q-machine experiments with cylindrical symmetries.

The turbulent transport in the Blaamann device is inherently 'bursty' in nature, and no diffusion limit [42, 57, 58] is established in the present conditions. The typical size of a density perturbation is not small compared with the scale length $\overline{n}/(\mathrm{d}\overline{n}/\mathrm{d}r)$ of the average plasma density. A locally homogeneous two dimensional turbulent region is not established, as it would be required for a universal spectral range to develop. A diffusion model therefore does not represent the proper physical process, but a quantity having the dimension of a diffusion coefficient can nonetheless be constructed as $D_{\text{eff}} \equiv \langle\Gamma_x\rangle/(\mathrm{d}\overline{n}/\mathrm{d}r)$, and is often used for characterizing the turbulent losses. In our case we have the numerical values $\langle\Gamma_x\rangle \approx 9.5 \times 10^{18}\,\mathrm{m}^{-2}\,\mathrm{s}^{-1}$, $\overline{n}/(\mathrm{d}\overline{n}/\mathrm{d}r) \approx 0.1\,\mathrm{m}$, and find $D_{\text{eff}} \approx 6.3\,\mathrm{m}^2\,\mathrm{s}^{-1}$, a number that turns out to be of the same order of magnitude as the Bohm diffusion coefficient for the present plasma parameters [30]. The effective diffusion coefficient is much larger than the result obtained for collisional or classical diffusion.

We have already commented on the similarity between our observed PDF's for the turbulent flux in a toroidal device and the results found in other linear devices [1, 2, 5, 40]. Since these flux-PDF's seem to have universal properties, it would be interesting to compare also our observed joint probability densities shown in figure 11 with results from other devices. If a similarity is found also for this case we can argue that some universal features can be attributed also to the excess statistics summarized in figures 12 and 13 since these results are contained in the joint PDFs for fluxes and their time derivatives $P(\Gamma_x, \Gamma'_x)$, as discussed in section 5.1.

Acknowledgments

The present data-sets were obtained in the Blaamann device at the Auroral Observatory of the University of Tromsø. The experiment has now been dismantled on the request of the Norwegian National Science Foundation. We would like to thank colleagues, students, and the technical staff for their contributions to the work on this experiment. In particular, we thank Terje Brundtland for his enthusiasm and tireless work in the construction and maintenance of the device. We thank Professor Helge Skullerud for discussion on the collisional cross-sections in the Blaamann plasma. Bjørn Lybekk was most helpful with the preparations of the manuscript.

References

[1] Huld T, Iizuka S, Pécseli H L and Juul Rasmussen J 1988 Experimental investigation of flute-type electrostatic turbulence *Plasma Phys. Control. Fusion* **30** 1297–318
[2] Nielsen A H, Pécseli H L and Juul Rasmussen J 1992 Vortex structures generated by the Kelvin-Helmholtz instability *Ann. Geophys.* **10** 655–67
[3] Liewer P C 1985 Measurements on microturbulence in Tokamaks and comparison with theories of turbulence and anomalous transport *Nucl. Fusion* **25** 543–621
[4] D'Ippolito D A, Myra J R and Zweben S J 2011 Convective transport by intermittent blob-filaments: comparison of theory and experiment *Phys. Plasmas* **18** 060501
[5] Huld T, Nielsen A H, Pécseli H L and Juul Rasmussen J 1991 Coherent structures in two-dimensional turbulence *Phys. Fluids* B **3** 1609–25
[6] Riccardi C and Fredriksen Å 2001 Waves and coherent structures in the turbulent plasma of a simple magnetized torus *Phys. Plasmas* **8** 199–209

[7] Fredriksen Å, Riccardi C, Cartegni L and Pécseli H 2003 Coherent structures, transport and intermittency in a magnetized plasma *Plasma Phys. Control. Fusion* **45** 721–33

[8] Fredriksen Å, Riccardi C and Magni S 2006 Effects of edge dc biasing on plasma rotation and transport in a toroidal geometry *Phys. Scr.* **T122** 11–14

[9] Nielsen A H, Pécseli H L and Juul Rasmussen J 1996 Turbulent transport in low-β plasmas *Phys. Plasmas* **3** 1530–44

[10] Johnsen H, Pécseli H L and Trulsen J 1987 Conditional eddies in plasma turbulence *Phys. Fluids* **30** 2239–54

[11] Filippas A V, Bengston R D, Li G X, Meier M, Ritz C P and Powers E J 1995 Conditional analysis of floating potential fluctuations at the edge of the Texas experimental tokamak upgrade (TEXT-U) *Phys. Plasmas* **2** 839–45

[12] Øynes F J, Olsen O-M, Pécseli H L, Fredriksen Å and Rypdal K 1998 Experimental study of low-frequency electrostatic fluctuations in a magnetized toroidal plasma *Phys. Rev.* E **57** 2242–55

[13] Grulke O, Klinger T and Piel A 1999 Experimental study of the dynamics of conditionally averaged structures in weakly developed electrostatic turbulence *Phys. Plasmas* **6** 788–96

[14] Trasarti-Battistoni R, Draghi D, Riccardi C and Roman H E 2002 Self-similarity, power-law scaling and non-Gaussianity of turbulent fluctuation flux in a nonfusion magnetoplasma *Phys. Plasmas* **9** 3369–77

[15] Fredriksen Å, Pécseli H L and Trulsen J 2008 Crash and recovery of the potential in a toroidal plasma column, as observed by generalized conditional sampling *New J. Phys.* **10** 033030

[16] Windisch T, Grulke O, Naulin V and Klinger T 2011 Intermittent transport events in a cylindrical plasma device: experiment and simulation *Plasma Phys. Control. Fusion* **53** 085001

[17] Zweben S J 1985 Search for coherent structure within tokamak plasma turbulence *Phys. Fluids* **28** 974–82

[18] Pierre T, Escarguel A, Guyomarc'h D, Barni R and Riccardi C 2004 Radial convection of plasma structures in a turbulent rotating magnetized-plasma column *Phys. Rev. Lett.* **92** 065004

[19] Barni R, Riccardi C, Pierre T, Leclert G, Escarguel A, Guyomarc'h D and Quotb K 2005 Formation of spiral structures and radial convection in the edge region of a magnetized rotating plasma *New J. Phys.* **7** 225

[20] Yamada T *et al* 2008 Anatomy of plasma turbulence *Nature Phys.* **4** 721–5

[21] Pécseli H L, Juul Rasmussen J and Thomsen K 1984 Nonlinear interaction of convective cells in plasmas *Phys. Rev. Lett.* **52** 2148–51

[22] Pécseli H L, Rasmussen J J, Sugai H and Thomsen K 1984 Evolution of externally excited convective cells in plasmas 1984 *Plasma Phys. Control. Fusion* **26** 1021–34

[23] Boedo J A *et al* 2003 Transport by intermittency in the boundary of the DIII-D tokamak *Phys. Plasmas* **10** 1670–7

[24] Xu Y H, Jachmich S, Weynants R R and TEXTOR-team 2005 On the properties of turbulence intermittency in the boundary of the TEXTOR tokamak *Plasma Phys. Control. Fusion* **47** 1841–55

[25] Spada E *et al* 2001 Search of self-organized criticality processes in magnetically confined plasmas: hints from the reversed field pinch configuration *Phys. Rev. Lett.* **86** 3032–5

[26] Fredriksen Å, Riccardi C, Cartegni L, Draghi D, Trasarti-Battistoni R and Roman H E 2003 Statistical analysis of turbulent flux and intermittency in the nonfusion magnetoplasma Blaamann *Phys. Plasmas* **10** 4335–40

[27] Magni S, Roman H E, Barni R, Riccardi C, Pierre T and Guyomarc'h D 2005 Statistical analysis of correlations and intermittency of a turbulent rotating column in a magnetoplasma device *Phys. Rev.* E **72** 026403

[28] Kervalishvili G N, Kleiber R, Schneider R, Scott B D, Grulke O and Windisch T 2008 Intermittent turbulence in the linear VINETA device *Contrib. Plasma Phys.* **48** 32–6

[29] Pécseli H L and Trulsen J 1991 Analytical expressions for conditional averages: a numerical test *Phys. Scr.* **43** 503–7

[30] Rypdal K, Grønvoll E, Øynes F, Fredriksen Å, Armstrong R J, Trulsen J and Pécseli H L 1994 Confinement and turbulent transport in a plasma torus with no rotational transform *Plasma Phys. Control. Fusion* **36** 1099–114

[31] Rypdal K, Garcia O E and Paulsen J V 1997 Anomalous cross-field current and fluctuating equilibrium of magnetized plasmas *Phys. Rev. Lett.* **79** 1857–60

[32] Pécseli H L, Mikkelsen T and Larsen S E 1983 Drift wave turbulence in a low-β plasma *Plasma Phys.* **25** 1173–97

[33] Kelley M C and Mozer F S 1973 Electric field and plasma density oscillations due to the high-frequency Hall current two-stream instability in the Auroral E region *J. Geophys. Res.* **78** 2214–21

[34] Kent G I, Jen N C and Chen F F 1969 Transverse Kelvin-Helmholtz instability in a rotating plasma *Phys. Fluids* **12** 2140–51

[35] Odajima K 1978 Effects of radial electric-field on drift wave instability in a weakly ionized plasma. *J. Phys. Soc. Japan* **44** 1685–93

[36] Pécseli H L 1982 Drift-wave turbulence in low-β plasmas *Phys. Scr.* **T2/1** 147–57

[37] Rypdal K and Ratynskaia S 2003 Statistics of low-frequency plasma fluctuations in a simple magnetized torus *Phys. Plasmas* **10** 2686–95

[38] Greiner F, Block D and Piel A 2004 Observation of mode like coherent structures in curved magnetic fields of a simple magnetized torus *Contrib. Plasma Phys.* **44** 335–46

[39] Chen F F 1979 Axial eigenmodes for long-$\lambda_\parallel$ waves in plasmas bounded by sheaths *Phys. Fluids* **22** 2346

[40] Nagashima Y *et al* 2011 Non-Gaussian properties of global momentum and particle fluxes in a cylindrical laboratory plasma *Phys. Plasmas* **18** 070701

[41] Rollefson J P 1978 On Kolmogorov's theory of turbulence and intermittency *Can. J. Phys.* **56** 1426–41

[42] Davidson P A 2004 *Turbulence. An Introduction for Scientists and Engineers* (Oxford: Oxford University Press)

[43] Krane B, Christopher I, Shoucri M and Knorr G 1998 Suppression of coherent structures in sheared plasma flows *Phys. Rev. Lett.* **80** 4422–5

[44] Tsuchiya H, Itoh S-I, Fujisawa A, Kamataki K, Shinohara S, Yagi M, Kawai Y, Komori A and Itoh K 2008 Sheared flow generation and mode suppression in a magnetized linear cylindrical plasma *Plasma Phys. Control. Fusion* **50** 055005

[45] Kristensen L, Casanova M, Courtney M S and Troen I 1991 In search of a gust definition *Boundary-Layer Meteorol.* **55** 91–107

[46] Rice S O 1945 Mathematical analysis of random noise: II *Bell System Tech. J.* **24** 46–156 (reprinted by Wax N 1954) *Selected Papers on Noise and Stochastic Processes* (New York: Dover)

[47] Yura H T and Hanson S G 2010 Mean level signal crossing rate for an arbitrary stochastic process *J. Opt. Soc. Am.* A **27** 797–807

[48] Sato H, Pécseli H L and Trulsen J 2012 Fluctuations in the direction of propagation of intermittent low frequency ionospheric waves *J. Geophys. Res.* **117** A03329

[49] Bendat J S 1958 *Principles and Applications of Random Noise Theory* (New York: Wiley)

[50] Block D, Teliban I, Greiner F and Piel A 2006 Prospects and limitations of conditional averaging *Phys. Scr.* **T122** 25–33

[51] Cheng J *et al* 2010 Statistical characterization of blob turbulence across the separatrix in HL-2A tokamak *Plasma Phys. Control. Fusion* **52** 055003
[52] Kono M and Tanaka M Y 2000 Spiral structures in magnetized rotating plasmas *Phys. Rev. Lett.* **84** 4369–72
[53] Fasoli A *et al* 2010 Electrostatic instabilities, turbulence and fast ion interactions in the TORPEX device *Plasma Phys. Control. Fusion* **52** 124020
[54] Furno I, Theiler C, Lançon D, Fasoli A, Iraji D, Ricci P, Spolaore M and Vianello N 2011 Blob current structures in TORPEX plasmas: experimental measurements and numerical simulations *Plasma Phys. Control. Fusion* **53** 124016
[55] Adrian R J 1979 Conditional eddies in isotropic turbulence *Phys. Fluids* **22** 2065–70
[56] Pécseli H L and Trulsen J 1989 A statistical analysis of numerically simulated plasma turbulence *Phys. Fluids* B **1** 1616–36
Pécseli H L and Trulsen J 1990 *Phys. Fluids* B **2** 454
[57] Taylor J B and McNamara B 1971 Plasma diffusion in two dimensions *Phys. Fluids* **14** 1492–9
[58] Misguich J H, Balescu R, Pécseli H L, Mikkelsen T, Larsen S E and Qiu Xiaoming 1987 Diffusion of charged particles in turbulent magnetoplasmas *Plasma Phys. Control. Fusion* **29** 825–56